

Article

## Defect-Driven Restructuring of TiO<sub>2</sub> Surface and Modified Reactivity Toward Deposited Gold Atoms

Kenneth Park <sup>1,\*</sup>, Vincent Meunier <sup>2</sup>, Minghu Pan <sup>3</sup> and Ward Plummer <sup>4</sup>

<sup>1</sup> Department of Physics, Baylor University, Waco, TX 76798, USA

<sup>2</sup> Department of Physics, Applied Physics, and Astronomy, Rensselaer Polytechnic Institute, Troy, NY 12180, USA; E-Mail: meuniv@rpi.edu

<sup>3</sup> Center of Nanophase Materials Sciences, Oak Ridge National Laboratory, TN 37831, USA; E-Mail: panm@ornl.gov

<sup>4</sup> Department of Physics and Astronomy, Louisiana State University, Baton Rouge, LA 70803, USA; E-Mail: wplummer@phys.lsu.edu

\* Author to whom correspondence should be addressed; E-Mail: Kenneth\_Park@baylor.edu; Tel.: +1-254-710-2282; Fax: +1-254-710-3878.

Received: 11 January 2013; in revised form: 17 February 2013 / Accepted: 19 February 2013 / Published: 8 March 2013

---

**Abstract:** A partially reduced TiO<sub>2</sub> surface exhibits increasingly complex nature when forming various defects, whose stoichiometry, structure and properties are markedly different from those of bulk TiO<sub>2</sub>. Using scanning tunneling microscopy and density functional theory, we investigate different types of surface defects formed by Ti interstitials on TiO<sub>2</sub> (110) and their reactivity toward deposited gold atoms. Sub-stoichiometric strands greatly enhance bonding of Au by transferring the excess charges from the reduced Ti<sup>3+</sup> onto the strands. Thus the sub-stoichiometric strands behave as strong electron donor sites toward reactants. On the contrary, fully stoichiometric nanoclusters provide increased Au bonding through its 1-coordinated oxygen, which acts as a strong electron acceptor site. Specific interactions between Au and defects as well as the implication of electron donor/acceptor complexes for catalytic reactions are discussed.

**Keywords:** TiO<sub>2</sub>; gold nanoclusters; STM; DFT

---

### 1. Introduction

Titanium dioxide, a simple binary compound, possesses a long list of intriguing surface properties [1,2]. Some of the well-known examples include photo-splitting of water [3], photo-degradation of organic molecules [4–6], and enhanced catalytic reactivity of gold nanoparticles supported on  $\text{TiO}_2$  [7–9]. Because defects play a crucial role in photochemistry and in heterogeneous catalysis, these phenomena have been attributed to the unique surface or interfacial structure and properties imparted by defects.

Among intrinsic defects, oxygen vacancy has been the focus of intense investigations on reduced surfaces of  $\text{TiO}_2$  [10–13]. It may be regarded as the simplest form of surface defects, created upon the loss of oxygen. However, a growing number of experiments have indicated that the presence of oxygen vacancy is not the only major characteristics of reduced  $\text{TiO}_2$  surfaces. Besides oxygen vacancy, the experimental and theoretical studies all point to the significance of Ti interstitials and their role in forming surface defects during re-oxidation [14–17]. The formation of such defects driven by Ti interstitials and the dynamic restructuring of the surface can have profound influence on chemical reactivity of partially reduced and re-oxidized  $\text{TiO}_2$  surface.

Bulk-like terminated  $\text{TiO}_2$  (110) surfaces constitute an interesting case study. On these systems, it is now established that the linear defects observed on  $(1 \times 1)$  terraces are sub-stoichiometric species (Figure 1(a)). The linear defects can be characterized as either single or double strands depending on the local stoichiometry of  $\text{TiO}$  or  $\text{Ti}_2\text{O}$ , respectively [18]. They can further assemble into  $(1 \times 1)$  or  $(1 \times 2)$  reconstructed surfaces. Either single or double strands can form depending on the local stoichiometry of  $\text{TiO}$  or  $\text{Ti}_2\text{O}$ , respectively. The proposed structural models (based on STM and DFT calculations) for the sub-stoichiometric defects have been independently confirmed by a high resolution TEM study [19].

As these sub-oxide species possess structures that are markedly different from that of the mother compound, a partially reduced surface of  $\text{TiO}_2$ , even in a single crystal model system, can become increasingly complex and heterogeneous. However, these sub-stoichiometric defects possess distinctive structural features that are easily identifiable on bulk-like terminated surfaces. First, sub-stoichiometric defects on (110) surface are all aligned along the particular crystallographic direction [001] forming strands (Figure 1(b)). In this geometry, a Ti row of a linear defect is sandwiched between the oxygen rows of the defect and the surface. As a result, the coordination number of Ti in the linear defect is kept as five like in stoichiometric surface despite a lower ratio of O to Ti [18]. Second, whether they are single or double strands, and whether isolated or assembled to form a reconstructed surface, the apparent height of the linear defect is approximately 1.6 Å corresponding to half-step height on (110). This value is a direct consequence of forming face-sharing oxygen octahedra at the interface between the defects and the substrate. Similar face-sharing oxygen octahedra are well known in reduced  $\text{TiO}_{2-x}$  bulk phases, for example at the crystallographic shear planes (CSP) of the  $\text{Ti}_2\text{O}_{2n-1}$  [20] as well as the corundum  $\text{Ti}_2\text{O}_3$  [1].

In addition to the sub-stoichiometric defects, partially reduced surfaces of  $\text{TiO}_2$  show another type of defects: a nanometer-sized, bright dot [21]. It is imaged by STM as a 3 Å high protrusion on (110) surface (Figure 1(a),(b)). Furthermore, it spans across both Ti (bright) and O (dark) rows of the terrace along [1–10], resulting in circular or elliptical shape as seen in STM images. Being topographically distinct from the linear sub-stoichiometric defect, the dots are ascribed as stoichiometric  $\text{TiO}_2$  nanoclusters with low coordination numbers. These topographical features of various types of defects

make it possible to discriminate between them by scanning tunneling microscopy (STM). It follows that a partially reduced TiO<sub>2</sub> (110) provides an exciting opportunity to probe nanometer-sized defects with well-defined, local stoichiometry and structures and their chemical reactivity. In this paper, we present a comparative study of various defects formed on TiO<sub>2</sub> (110)—both sub-stoichiometric and stoichiometric—and their role as the nucleation sites for the initial adsorption of Au using STM and density functional theory (DFT).

## 2. Results and Discussion

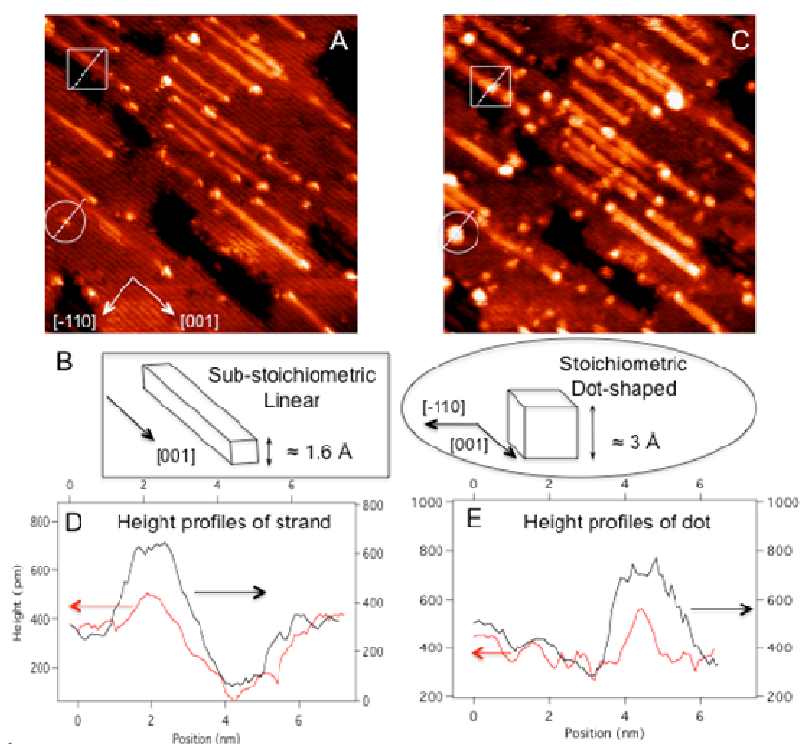
A typical STM image of reduced TiO<sub>2</sub> (110) showed that 5% of the surface area was covered by sub-stoichiometric strands (Figure 1(a)). After one minute of Au deposition, numerous bright clusters are observed on partially reduced TiO<sub>2</sub> (110) (Figure 1(c)). The large clusters have diameters of about 20 Å and heights of 5 Å on average. The comparison of the same area before and after Au deposition clearly shows that many of the large Au cluster formation started preferentially with pre-existing defects such as strands (highlighted by squares), their end structures, and dots on (1 × 1) terraces (highlighted in circles). Because these native defects already have significant heights (e.g., 1.5 Å to 3 Å tall) and widths, only the part of measured heights and widths can be assigned to adsorbed Au clusters. For example, the comparison in height profiles of the strand defect between before and after Au deposition reveals that only one layer thick Au cluster is adsorbed on top of the strand (Figure 1(d)). Similarly for the dot defect, the height increased from 3 Å to 5 Å upon Au deposition, indicating that the adsorbed Au cluster is one monolayer thick (Figure 1(e)). However, the full-width-at-half-maximum (FWHM) of the defect also increased deposition along [−110] from 8 Å to 20 Å, suggesting that the Au cluster grew laterally as well to form a quasi-2D raft with the height of 2 atomic layers.

In addition to large clusters, smaller clusters having diameters of about 7 Å and heights of 2 Å are also observed. They appear to be scattered at various sites, including strands, their ends, and step edges as well as on (1 × 1) terraces, presumably at oxygen vacancies or sites near sub-surface Ti interstitials. Because these small Au clusters have similar topographical features as the native stoichiometric dot defects, it would be a non-trivial task to distinguish them from native defects. However, the comparison of the same area used in this study allows one to unambiguously identify them as Au clusters. Counting all the Au clusters, the total surface coverage of Au on TiO<sub>2</sub> (110) is estimated as 0.02 monolayers (ML), where 1 ML is equal to  $1.39 \times 10^{15}$  atoms/cm<sup>2</sup>. Using a larger data set, 69% of the new Au clusters are observed at the dot defects (including the end structures of the strands), 14% are at or on the side of line defects, and 17% are on seen on the (1 × 1) terraces, presumably on top of O vacancy sites.

For the investigation of the energetics of defect-structures of TiO<sub>2</sub> and subsequent Au adsorption, theoretical modeling was performed using VASP package based on DFT [22–24]. The calculations were carried out using a slab model keeping the atoms of the bottom layers at bulk positions to simulate the semi-infinite crystal. The unit cells had the following lateral dimensions:  $1.119 \times 1.317$  nm<sup>2</sup> for Au on a linear defect and  $1.783 \times 1.317$  nm<sup>2</sup> for Au on a nanocluster defect. In the direction perpendicular to the slab the dimension was chosen to ensure a 1.5 nm vacuum between images. Core atomic states were represented by projector augmented wave pseudopotentials [25,26] within the

Perdew-Wang (PW91) generalized gradient approximation (GGA) for the exchange-correlation functional [27]. For selected systems, the calculations were also performed using the Perdew-Burke-Ernzerhof (PBE) GGA functional [28] and spin polarization in order to verify the main results associated with the energetics of adsorption. Plane-wave basis with energy cut-off up to 400 eV, a fine k-point sampling of the surface Brillouin zone were chosen after careful convergence studies of the total energy. For each structure energy convergence down to 0.1 meV and forces smaller than 4 meV/Å were systematically reached.

**Figure 1.** (A) STM scan of a  $40 \times 40 \text{ nm}^2$  area of  $(1 \times 1)$   $\text{TiO}_2$  (110) with full of defects; (B) schematic diagrams of substoichiometric strand and stoichiometric dot defects contrasting their distinct topographical features; (C) STM scan of the same area in (A) after 1 min Au deposition at room temperature ( $\approx 0.02 \text{ ML}$ ). The height profiles, across (D) the strand and (E) the dot defects ((highlighted in squares and circles, respectively), reveal a marked increase in the height as well as the FWHM along  $[-110]$  (along the dotted lines) due to Au adsorption. The height profiles before and after Au adsorption are shown in red and black lines, respectively. Both STM scans are taken with  $V = 1.80 \text{ V}$  and  $I = 0.5 \text{ nA}$  for (A) and  $V = 1.42 \text{ V}$  and  $0.5 \text{ nA}$  for (C).



The initial adsorption of Au is examined on the strand and dot defects by comparing the energetics at various sites. The adsorption energy for Au is defined as the difference in the total energy before and after Au attachment per unit cell,  $E_A = E(\text{Au}/\text{TiO}_2) - [E(\text{TiO}_2) + E(\text{Au})]$ . As for a reference, the adsorption energy of an Au atom above a 2-coordinated oxygen (2c-O, also known as a bridging oxygen) on stoichiometric  $\text{TiO}_2$  (110) is calculated using two differently functionals. The calculated values of  $-0.64 \text{ eV}$  with PBE and  $-0.57 \text{ eV}$  with PW91 are in good agreement with the reported value of  $-0.61 \text{ eV}$  [29].

For the Au adsorption on the strands, the linear defect is modeled as a single strand ( $\text{Ti}_2\text{O}_2$ ) [18]. The energetically most favorable site for a single Au atom is found at the hollow site, 2.73 Å and 2.75 Å away from the two nearest 5c-Ti atoms and 3.00 Å and 3.03 Å from the two O atoms in-plane with the Ti atoms (Figure 2(a),(b)). Upon the Au adsorption, the strand undergoes a substantial structural relaxation. The two 5c-Ti atoms are pulled toward each other while the two O atoms are slightly pushed apart (Figure 2(c)). The adsorption energy for Au on the single strand is calculated as  $-3.11$  eV, representing an exceptionally strong bonding between the Au atom and  $\text{TiO}_2$  (110) via the strand defect. The large enhancement in bonding is also accompanied by a significant amount of charge transfer from the strand to the adsorbed Au atom. Using Bader's charge analysis [30,31], it is calculated that Au acquires  $0.54 e^-$  upon adsorption and becomes negatively charged.

The effect of the sub-stoichiometric strand on Au bonding is qualitatively in good agreement with recent DFT calculations of reporting similar effects of electron donor defects on Au adsorption on  $\text{TiO}_2$  (110). Madsen and Hammer [32] reported that the presence of a sub-surface Ti interstitial significantly enhances the bonding of Au on otherwise, defect-free  $\text{TiO}_2$  (110). The energy of Au on  $\text{TiO}_2$  (110) was lowered by about 1 eV with the Ti interstitial defect, and Au gained about  $0.3 e^-$  regardless of the types of functionals. They further concluded that other types of sub-surface defects, such as oxygen vacancy and CSP, had the same effect on Au bonding on surface. Similarly, Chrétien and Metiu [33] reported that co-adsorption of electron donating molecules as well as artificial addition of an extra electron increase the binding energy of an Au atom on 5c-Ti increased from 0.45 eV for defect-free  $\text{TiO}_2$  (110) to  $1.2 < 1.3$  eV. However, the very large enhancement in bonding and charge accumulation at Au observed in this study is unique to the strand defect by its sub-stoichiometric and spatially extended nature. Although the Ti atoms underneath the Au atom exhibit the largest change in charge by  $0.021 e^-$ , all the Ti atoms around the adsorbed Au as well as sub-surface Ti atoms contribute to the charge transfer. The spatial map of difference in valence charge density clearly shows the extended nature of charge transfer not only along the strand but also into sub-surface, providing exceptional stability of Au atom (Figure 2(d)).

**Figure 2.** DFT-relaxed structure of Au adsorbed on the sub-stoichiometric strand defect on  $\text{TiO}_2$  (110) viewed along (a) [001], (b) [1-10], and (c) [-1-10] (Au: yellow, Ti: blue; O: red). (d) The charge density difference isosurface plot of (b) revealing electron surplus (blue) and depletion (yellow).

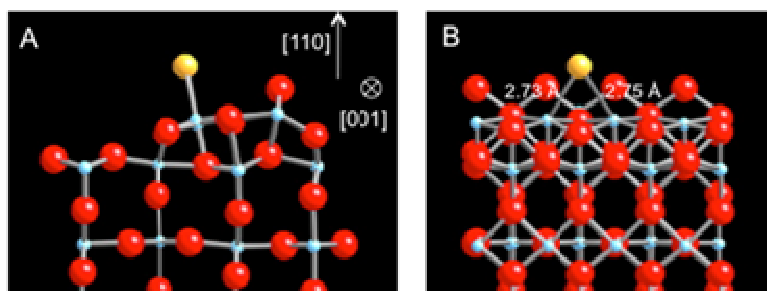
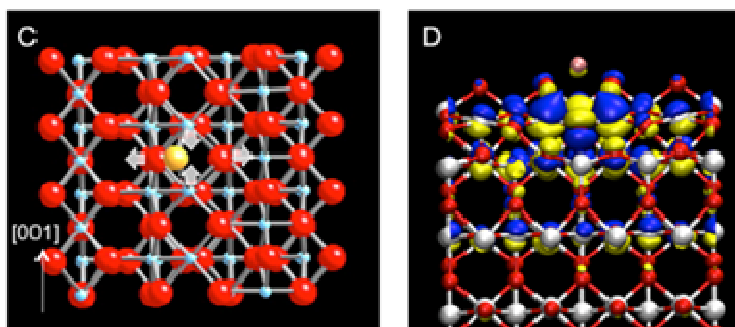
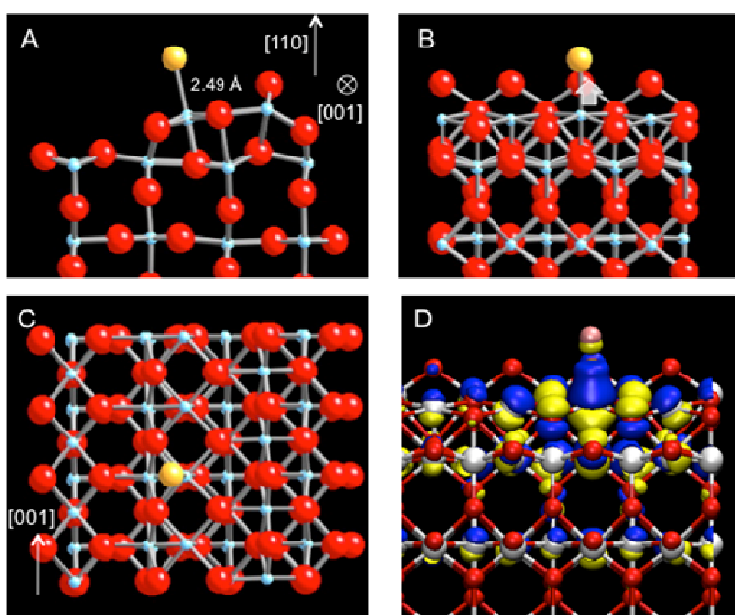


Figure 2. Cont.



The participation of neighboring Ti atoms in Au bonding further suggests that the variation in energetics of Au adsorption along the strand may be relatively small. Indeed, there is another energetically favorable site for the Au atom, displaced approximately by half the lattice constant along [001]. The Au atom is directly located at 2.49 Å above the 5-coordinated Ti (5c-Ti) of the linear defect (Figure 3(a)–(c)). The adsorption energy at the top site is  $-2.91$  eV, the difference of only 200 meV compared to the previous hollow site. Upon the Au adsorption, the strand also undergoes a structural relaxation. In particular, the 5c-Ti is pulled up toward the Au atom, increasing its bond distance to the oxygen underneath from 1.95 Å to 2.12 Å (Figure 3(b)). The isosurface map of charge density difference shows the electron accumulation along the bond axis between Ti and Au as the major effect but also clearly reflects the delocalized nature of charge density variation along the strand for this adsorption site as well (Figure 3(d)). As the energetics of the Au atom is predominantly influenced by the Ti 4d states with large dispersion along [001], the adsorbed Au is expected to diffuse easily along the strand, analogous to a facile diffusion of Au on  $\text{TiO}_2$  (110) along the Ti trough [29].

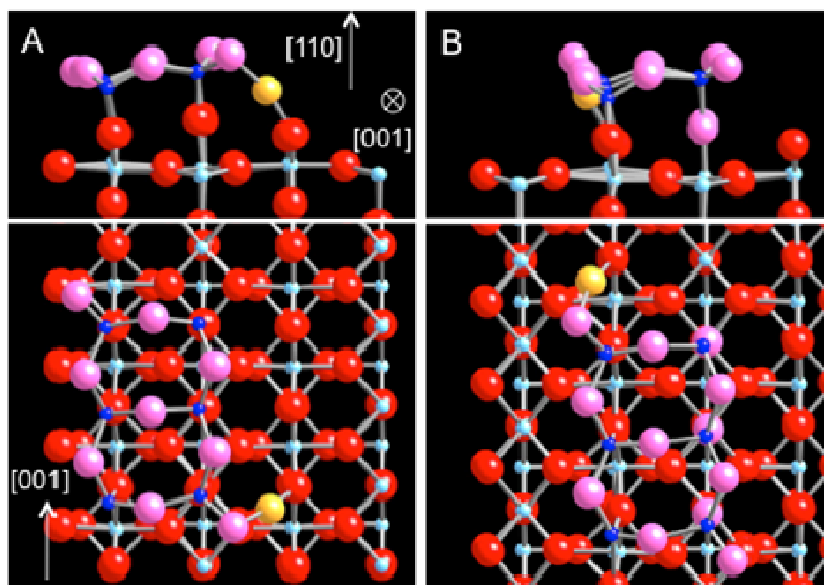
**Figure 3.** DFT-relaxed structure of Au adsorbed at an alternative site on the sub-stoichiometric strand defect viewed along (a) [001], (b) [1–10], and (c) [–1–10] (Au: yellow, Ti: blue; O: red). (d) The charge density difference isosurface plot of (b) revealing electron surplus (blue) and depletion (yellow).



Another type of surface defects at which Au atoms adsorb and nucleate, is expressed as a bright dot. The strand defect is usually terminated with the dots as the end structure. However, the dots are also observed as isolated alone on a terrace. Because in both cases, the dots exhibit the same topographical features and reactivity toward Au, the initial adsorption of Au on a dot is investigated with a fully stoichiometric nanocluster of  $(\text{TiO}_2)_6$  isolated on  $(1 \times 1)$   $\text{TiO}_2$  (110) [21].

The energetically most favorable position for the gold adsorption site is found between the 1c-O atom of the nanocluster defect and the surface 2c-O atom (Figure 4(a)). The adsorption energy for the Au atom at the cluster defect is calculated as  $-2.74$  eV using either PW91 or PBE. The large adsorption energy can be understood from the unique bond geometry and electronic structure the nanocluster provides for Au. The adsorbed Au atom is nearly at equidistance from the 1c-O atom of the nanocluster defect and the surface 2c-O atom,  $2.03$  Å and at  $2.05$  Å, respectively. Moreover, at the adsorption site substantial density of states derived from O 2p are available just above the Fermi level. Ordinarily for rutile  $\text{TiO}_2$ , the O 2p states are mainly occupied forming the valence band, and the empty conduction band consists largely of the Ti 4d states. However, for the nanocluster defect, a part of the O 2p states is pushed up above the Fermi level due to Coulomb repulsion. The partially unoccupied states from the 1c-O of the cluster defect and the surface 2c-O become available for the hybridization with the Au 6s state. In this case, the Au atom loses about  $0.2 e^-$ , which are redistributed mostly to the two oxygen atoms. It follows that the enhancement of Au bonding originates from the lowering of the energy due to the hybridization between the two types of O atoms along with a lowering of the Coulomb repulsion by having the Au adsorption site between the defect and surface O atoms.

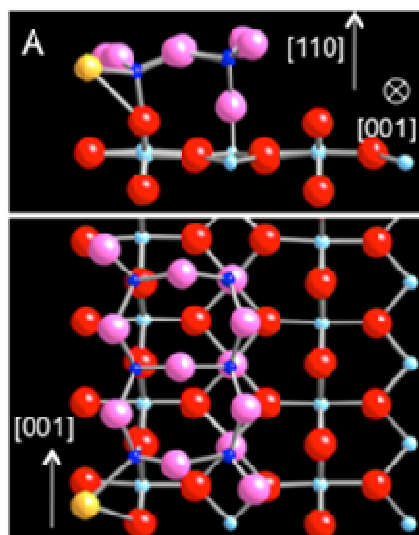
**Figure 4.** DFT-relaxed structures of Au adsorbed on the dot defect, modeled as  $(\text{TiO}_2)_6$  on  $\text{TiO}_2$  (110). (a) The energetically most favorable site and (b) the alternative 1-coordinated O site. At both locations, Au is found between the 1c-O of the defect and the 2c-O of the surface. Au becomes anionic, losing electrons to the oxygen atoms of low coordination (defect Ti: dark blue; defect O: pink).



There is another 1-c O atom at the opposite end of the cluster defect (Figure 4(b)). This site would be equivalent to the previous site if one considered the cluster geometry alone. However this site is located next to the 5-c Ti rows of the surface, thus breaking the symmetry. The Au atom bonds to the 1-c O atom of the  $(\text{TiO}_2)_6$  nanocluster and the 2-c O atom of the surface with nearly the same bond lengths of 2.02 Å. The adsorption energy (using the PW91 functional) is calculated as  $-2.10$  eV for this site. Although this site is energetically less stable than the previous site by 0.64 eV, the enhancement of Au bonding is based on the same mechanism: the hybridization between the partially unoccupied O 2p states and the Au 6s state to facilitate charge transfer. Then, the wedge sites around the nanocluster defect, i.e. between the 1c-O of the nanocluster and the 2c-O of the surface, may be viewed as an electron acceptor center, whereas the strand defect as a strong electron donor site with its ability to reduce adsorbates.

In addition to the O atoms of low coordination, the nanocluster of  $(\text{TiO}_2)_6$  also possesses a 3-c Ti atom. The stable adsorption site for Au is found at 2.57 Å from the 3-c Ti atom (Figure 5). The adsorbed Au atom is also coordinated to the 2-c O atom of the surface at 2.98 Å away in a similar manner observed for the Au in Figure 4(b). The bond distances are much larger than those observed at the previous sites: 2.49 Å for Au-Ti and  $2.02 \approx 2.05$  Å for Au-O, reflecting a much smaller interaction at the adsorption site. Indeed, the adsorption energy for this site is calculated as  $-1.37$  eV, significantly smaller than those for the previous two sites, where the Au atom is coordinated to both O atoms of the defect and the surface.

**Figure 5.** DFT calculation of Au adsorbed at the 3-coordinated Ti site of the dot defect, modeled as  $(\text{TiO}_2)_6$  on  $\text{TiO}_2$  (110).



The comparable bond enhancement of Au observed at both stoichiometric and sub-stoichiometric defects suggests that they may compete for the formations of cationic and anionic  $\text{Au}^{-\delta}$  species for a given condition. Thus for low temperature CO oxidation, both types of defects and bond mechanisms must be carefully examined. However, considering a typical catalyst preparation via wet chemistry followed by heating in air, the stabilization of Au particles by stoichiometric nanoclusters may be favored over by the sub-stoichiometric, extended defects. In fact, the strong adsorption of Au at the

perimeter of the stoichiometric nanocluster defect is consistent with key characteristics, recently suggested for active gold species supported metal oxides. A number of experimental and theoretical studies have indicated that cationic Au species are the catalytically active form [34–41]. In particular, Camellone and Fabris [40] reported DFT calculations showing the selective adsorption of CO on positively charged Au and further proposed the formation of Au-COO\* with the closest lattice O atom of CeO<sub>2</sub>. We have separately shown that the positively charged Au<sub>3</sub> cluster formed at the nanocluster strongly binds CO with the adsorption energy of −1.11 eV [21].

Another common characteristics emerging from recent investigations is the presence of small Au particles (≤1 nm) identified in active catalyst samples only. Unlike the earlier belief of 2- to 5-nm Au particles as the most active form, a number of studies have now indicated the continued increase in the CO oxidation activity as the Au particle size decreases. Using aberration-corrected scanning transmission electron microscopy, Herzing *et al.* [41] highlighted the strong correlation between high catalytic activity of Au/FeO<sub>x</sub> for CO oxidation and the presence of bilayer clusters of <5 Å in diameter that contain about 10 Au atoms only. Likewise, Rashkeev *et al.* [42] reported evidence that most Au particles are only one to two layers thick in the most active form of Au/TiO<sub>2</sub> catalysts. The topographical features of quasi-2D Au rafts grown (Figure 1) in this model study are strikingly similar to the reported shapes and size for the active Au species supported on oxides. The interface between Au cluster and the stoichiometric nanocluster defect could well be the site, where the crucial step of the CO oxidation reaction takes place as envisioned by Haruta and co-workers [43].

### 3. Experimental Section

The experiments were carried out using a variable temperature STM in an ultrahigh vacuum (UHV) chamber with base pressure less than  $8 \times 10^{-11}$  Torr. Because a reduced TiO<sub>2</sub> (110) can become hydroxylated even under UHV [44], the surface was prepared with utmost care. A rutile TiO<sub>2</sub> (110) sample was cleaned by repeated cycles of sputtering and annealing. A typical sputtering cycle used Ar-ion bombardment ( $E < 1.5$  keV) with the ion currents of about 0.5 μA at the sample for 15 to 20 min. The Ar sputtering was immediately followed by annealing up to 650 °C for 15 min. The TiO<sub>2</sub> (110) surface used in this experiment underwent close to 100 cleaning cycles in total. The appearance of the sample changed progressively from transparent to blue and to deep blue.

Soon after obtaining (1 × 1) TiO<sub>2</sub> (110), gold was deposited at room temperature at the STM stage using an e-beam evaporator. The gold source was bombarded with electron beams of 15.0 mA at 700 V. The evaporation rate was monitored through the Au flux measured at the opening of the evaporator (≈42 nA). During the evaporation, the pressure remained below  $2 \times 10^{-10}$  Torr. For STM measurements, we used a constant current topographic mode. Sample biases were usually chosen between +1.0 and +2.2 V. All STM images presented here were obtained at room temperature.

### 4. Conclusions

In summary, the combined STM and DFT study presented in this paper points to the fact that TiO<sub>2</sub>, as a reducible oxide, can form both sub-stoichiometric and fully stoichiometric defects on surface, driven by Ti-interstitials. These defects can influence surface chemical reactivity with their distinct bonding geometry, local electronic structures, and charge re-distribution at various sites around the

defects. For gold chemisorption, bonding of Au is greatly enhanced at the sub-stoichiometric strand defect by electron transfer to Au and the formation of anionic  $\text{Au}^{\delta-}$ . All the Ti atoms in and around the strand participate in charge transfer. The strand as a whole behaves as an electron donor site. The enhancement of Au bonding is also observed at the fully stoichiometric nanocluster defect. However, the strongest enhancement comes from the wedge site between the 1c-O of the cluster and the 2c-O of the surface. With the partially unoccupied O 2p states, the electron is transferred from Au to the two O atoms forming cationic  $\text{Au}^{\delta+}$ , and the interaction is highly localized. The wedge site acts as a strong electron acceptor site. The exceptionally strong bonding of Au observed at both stoichiometric and sub-stoichiometric defects highlights the importance of surface restructuring driven by Ti interstitials and locally modified chemical reactivity.

### Acknowledgments

This research was sponsored by the Scientific User Facilities Division and also by the Division of Materials Science (DE AC05-00OR22725 contracted with UT-Battelle, LLC), Department of Energy. The computations were performed using the resources of the National Center for Computational Sciences at ORNL. One of us (EWP) was funded by DOE DE-SC0001058. Research at RPI (VM) was also sponsored in part by the Army Research Laboratory and was accomplished under Cooperative Agreement Number W911NF-12-2-0023.

### Conflict of Interest

The authors declare no conflict of interest.

### References

1. Henrich, V.E.; Cox, P.A. *The Surface Science of Metal Oxides*; Cambridge University Press: Cambridge, UK, 1994.
2. Diebold, U. The surface science of titanium dioxide. *Surf. Sci. Rep.* **2003**, *48*, 53–229.
3. Fujishima, A.; Honda, K. Electrochemical photolysis of water at a semiconductor electrode. *Nature* **1972**, *238*, 37–38.
4. Fox, M.A.; Dulay, M.T. Heterogeneous photocatalysis. *Chem. Rev.* **1993**, *93*, 341–357.
5. Mills, A.; Davies, R.H.; Worsley, D. Water-purification by semiconductor photocatalysis. *Chem. Soc. Rev.* **1993**, *22*, 417–425.
6. Linsebigler, A.L.; Lu, G.; Yates, J.T., Jr. Photocatalysis on  $\text{TiO}_2$  surfaces: Principles, mechanisms, and selected results. *Chem. Rev.* **1995**, *95*, 735–758.
7. Haruta, M.; Yamada, N.; Kobayashi, T.; Iijima, S. Gold catalysts prepared by coprecipitation for low-temperature oxidation of hydrogen and of carbon monoxide. *J. Catal.* **1989**, *115*, 301–309.
8. Valden, M.; Lai, X.; Goodman, D.W. Onset of catalytic activity of gold clusters on titania with the appearance of nonmetallic properties. *Science* **1998**, *281*, 1647–1650.
9. Meyer, R.; Lemire, C.; Shaikhutdinov, S.K.; Freund, H.-J. Surface chemistry of catalysis by gold. *Gold Bull.* **2004**, *37*, 72–124.

10. Wahlström, E.; Lopez, N.; Schaub, R.; Thostrup, P.; RØnnau, A.; Africh, C.; Lægsgaard, E.; NØrskov, J.K.; Besenbacher, F. Bonding of gold nanoclusters to oxygen vacancies on rutile TiO<sub>2</sub> (110). *Phys. Rev. Lett.* **2003**, *90*, 026101.
11. Schaub, R.; Wahlström, E.; RØnnau, A.; Lægsgaard, E.; Stensgaard, I.; Besenbacher, F. Oxygen-mediated diffusion of oxygen vacancies on the TiO<sub>2</sub> (110) surface. *Science* **2003**, *299*, 377–379.
12. Bikondoa, O.; Pang, C.L.; Ithnin, R.; Muryn, C.A.; Onishi, H.; Thornton, G. Direct visualization of defect-mediated dissociation of water on TiO<sub>2</sub> (110). *Nature* **2006**, *5*, 189–192.
13. Ganduglia-Pirovano, M.V.; Hofmann, A.; Sauer, J. Oxygen vacancies in transition metal and rare earth oxides: Current state of understanding and remaining challenges. *Surf. Sci. Rep.* **2007**, *62*, 219–270.
14. Onishi, H.; Iwasawa, Y. Dynamic visualization of a metal-oxide-surface/gas-phase reaction: Time-resolved observation by scanning tunneling microscopy at 800 K. *Phys. Rev. Lett.* **1996**, *76*, 791–794.
15. Henderson, M.A. Surface perspective on self-diffusion in rutile TiO<sub>2</sub>. *Surf. Sci.* **1999**, *419*, 174–187.
16. Bennett, R.A.; Stone, P.; Price, N.J.; Bowker, M. Two (1 × 2) reconstructions of TiO<sub>2</sub> (110): surface rearrangement and reactivity studied using elevated temperature scanning tunneling microscopy. *Phys. Rev. Lett.* **1999**, *82*, 3831–3834.
17. McCarty, K.F.; Bartelt, N.C. Role of bulk thermal defects in the reconstruction dynamics of the TiO<sub>2</sub> (110) surface. *Phys. Rev. Lett.* **2003**, *90*, 046104.
18. Park, K.T.; Pan, M.H.; Meunier, V.; Plummer, E.W. Surface reconstructions of TiO<sub>2</sub> (110) driven by suboxides. *Phys. Rev. Lett.* **2006**, *96*, 226105.
19. Shibata, N.; Goto, A.; Choi, S.-Y.; Mizoguchi, T.; Findlay, S.D.; Yamamoto, T.; Ikuhara, Y. Direct imaging of reconstructed atoms on TiO<sub>2</sub> (110) surfaces. *Science* **2008**, *322*, 570–573.
20. Bursill, L.A.; Hyde, B.G. Crystallographic shear in the higher titanium oxides: Structure, texture, mechanisms and thermodynamics. *Prog. Solid State Chem.* **1972**, *7*, 177–253.
21. Park, K.T.; Meunier, V.; Pan, M.H.; Shelton, W.A.; Yu, N.-H.; Plummer, E.W. Nanoclusters of TiO<sub>2</sub> wetted with gold. *Surf. Sci.* **2009**, *603*, 3131–3135.
22. Kresse, G.; Hafner, J. *Ab initio* molecular dynamics for liquid metals. *Phys. Rev. B* **1993**, *47*, 558–561.
23. Kresse, G.; Furthmüller, J. Efficiency of *ab-initio* total energy calculations for metals and semiconductors using a plane-wave basis set. *Comput. Mater. Sci.* **1996**, *6*, 15–50.
24. Kresse, G.; Furthmüller, J. Efficient iterative schemes for *ab initio* total-energy calculations using a plane-wave basis set. *Phys. Rev. B* **1996**, *54*, 11169–11186.
25. Blöchl, P.E. Projector augmented-wave method. *Phys. Rev. B* **1994**, *50*, 17953–17979.
26. Kresse, G.; Joubert, D. From ultrasoft pseudopotentials to the projector augmented-wave method. *Phys. Rev. B* **1999**, *59*, 1758–1775.
27. Perdew, J.P.; Chevary, J.A.; Vosko, S.H.; Jackson, K.A.; Pederson, M.R.; Singh, D.J.; Fiolhais, C. Atoms, molecules, solids, and surfaces: Applications of the generalized gradient approximation for exchange and correlation. *Phys. Rev. B* **1992**, *46*, 6671–6687.
28. Perdew, J.P.; Burke, K.; Ernzerhof, M. Generalized gradient approximation made simple. *Phys. Rev. Lett.* **1996**, *77*, 3865–3868.

29. Matthey, D.; Wang, J.G.; Wendt, S.; Matthiesen, J.; Schaub, R.; Lægsgaard, E.; Hammer, B.; Besenbacher, F. Enhanced bonding of gold nanoparticles on oxidized TiO<sub>2</sub> (110). *Science* **2007**, *315*, 1692–1696.
30. Bader, R.F.W. *Atoms in Molecules: A Quantum Theory*; Oxford University Press: Oxford, UK, 1990.
31. Henkelman, G.; Arnaldsson, A.; Jónsson, H. A fast and robust algorithm for Bader decomposition of charge density. *Comput. Mater. Sci.* **2006**, *36*, 354–360.
32. Madsen, G.K.H.; Hammer, B. Effect of subsurface Ti-interstitials on the bonding of small gold clusters on rutile TiO<sub>2</sub> (110). *J. Chem. Phys.* **2009**, *130*, 044704.
33. Chrétien, S.; Metiu, H. Enhanced adsorption energy of Au<sub>1</sub> and O<sub>2</sub> on the stoichiometric TiO<sub>2</sub> (110) surface by coadsorption with other molecules. *J. Chem. Phys.* **2008**, *128*, 044714.
34. Fu, Q.; Saltsburg, H.; Flytzani-Stephanopoulos, M. Active Nonmetallic Au and Pt species on ceria-based water-gas shift catalysts. *Science* **2003**, *301*, 935–938.
35. Guzman, J.; Gates, B.C. Catalysis by Supported Gold: Correlation between catalytic activity for CO oxidation and oxidation states of gold. *J. Am. Chem. Soc.* **2004**, *126*, 2672–2673.
36. Hutchings, G.J.; Hall, M.S.; Carley, A.F.; Landon, P.; Solsona, B.E.; Kiely, C.J.; Herzing, A.; Makkee, M.; Moulijn, J.A.; Overweg, A.; *et al.* Role of gold cations in the oxidation of carbon monoxide catalyzed by iron oxide-supported gold. *J. Catal.* **2006**, *242*, 71–81.
37. Haruta, M.; Daté, M. Advances in the catalysis of Au nanoparticles. *Appl. Catal. A* **2001**, *222*, 427–437.
38. Wu, X.; Senapati, L.; Nayak, S.K.; Selloni, A.; Hajaligol, M. A density functional study of carbon monoxide adsorption on small cationic, neutral, and anionic gold clusters. *J. Chem. Phys.* **2002**, *117*, 4010–4015.
39. Molina, L.M.; Hammer, B. Active role of oxide support during CO oxidation at Au/MgO. *Phys. Rev. Lett.* **2003**, *90*, 206102.
40. Camellone, M.F.; Fabris, S. Reaction mechanisms for the CO oxidation on Au/CeO<sub>2</sub> catalysts: activity of substitutional Au<sup>3+</sup>/Au<sup>+</sup> cations and deactivation of supported Au<sup>+</sup> adatoms. *J. Am. Chem. Soc.* **2009**, *131*, 10473–10483.
41. Herzing, A.A.; Kiely, C.J.; Carley, A.F.; Landon, P.; Hutchings, G.J. Identification of active gold nanoclusters on iron oxide supports for CO oxidation. *Science* **2008**, *321*, 1331–1335.
42. Rashkeev, S.N.; Luipini, A.R.; Overbury, S.H.; Pennycook, S.J.; Pantelides, S.T. Role of the nanoscale in catalytic CO oxidation by supported Au and Pt nanostructures. *Phys. Rev. B* **2007**, *76*, 035438.
43. Haruta, M. Catalysis of gold nanoparticles deposited on metal oxides. *CATTECH* **2002**, *6*, 102–115.
44. Wendt, S.; Schaub, R.; Matthiesen, J.; Vestergaard, E.K.; Wahlström, E.; Rasmussen, M.D.; Thostrup, P.; Molina, L.M.; Lægsgaard, E.; Stensgaard, I.; *et al.* Oxygen vacancies on TiO<sub>2</sub>(110) and their interaction with H<sub>2</sub>O and O<sub>2</sub>: A combined high-resolution STM and DFT study. *Surf. Sci.* **2005**, *598*, 226–245.